Arab J Sci Eng (2014) 39:2021–2031
DOI 10.1007/s13369-013-0767-y

RESEARCH ARTICLE - ELECTRICAL ENGINEERING

MPPT System for Photovoltaic Module Connected to Battery Adapted for Unstable Atmospheric Conditions Using VHDL-AMS

A. Ballouti · F. Djahli · A. Bendjadou · N. Belhaouchet · A. Benhamadouche

Received: 23 May 2012 / Accepted: 12 July 2013 / Published online: 12 September 2013

Abstract This paper presents a novel maximum power point tracking (MPPT) algorithm used in photovoltaic (PV) module connected to a storage battery. The main aim of this algorithm is to maximize the PV array output power by tracking continuously the maximum power point (MPP) which depends on atmospheric conditions (panel temperature and irradiance). The full system is composed of a PV array, a storage battery and an electronic boost-type DC–DC converter inserted between the PV array and the storage battery. The proposed MPPT control algorithm used to control the boost DC–DC converter is intended to lead the PV array power to its maximum point by keeping the PV array voltage stable with little deviation. The modeling of this system is realized using the novel concept of "functional prototyping" based on Very high speed integrated circuits Hardware Description language–Analog and Mixed Signal (VHDL-AMS) which can be particularly useful to design and redesign complex system with multi-technologic aspect, and to optimize strategies of control. The usefulness of the proposed MPPT algorithm has been fully verified by digital simulation using Simplorer software, where the obtained results show that the proposed MPPT method can improve PV power system performances noticeably in steady and dynamic states.

Keywords Photovoltaic (PV) · Maximum power point tracking (MPPT) · Functional prototyping · VHDL-AMS

A. Ballouti (✉) · F. Djahli · A. Bendjadou · A. Benhamadouche
Department of Electronics, Faculty of Technology, University of Setif 1, 19000 Maabouda Setif, Algeria
e-mail: Adelbb2002@yahoo.fr

N. Belhaouchet
Department of Electrotechnic, Faculty of Technology, University of Setif 1, 19000 Maabouda Setif, Algeria

الخلاصة

تعرض هذه الورقة العلمية خوارزمية جديدة لتتبع نقطة الاستطاعة العظمى (MPPT) المستخدمة في وحدة فوتوفولتية متصلة ببطارية تخزين. والهدف الرئيسي من هذه الخوارزمية هو تفخيم استطاعة مخرج اللوحة الشمسية الفوتوفولتية بتتبع دائم لنقطة الاستطاعة العظمى التي تتعلق بالأحوال الجوية (درجة الحرارة والإشعاع الشمسي). يتألف النظام من لوحة شمسية فوتوفولتية، وبطارية تخزين ومحول إلكتروني من النوع مستمر- مستمر رافع للتوتر كوسيط بين اللوحة الشمسية الفوتوفولتية وبطارية التخزين. إنّ الخوارزمية المقترحة لتتبع نقطة الاستطاعة العظمى التي بدورها تتحكم في المحول الإلكتروني مستمر- مستمر تهدف الى جعل اللوحة الشمسية الفوتوفولتية تعمل في نقطة استطاعتها العظمى وذلك بالمحافظة على توترها مستقر قدر الإمكان. إنّ نمذجة هذا النظام استخدمت بمفهوم جديد من "النموذج الخيالي" معتمدة على لغة توصيف سريعة للعتاد والدارات المتكاملة بأنظمة اشارات تماثلية-رقمية و مختلطة (AMS - VHDL) والتي بإمكانها أن تكون مفيدة بخاصة لتصميم وإعادة تصميم الأنظمة المركبة متعدد التكنولوجيات ولتحسين استراتيجيات التحكم. لقد تم التحقق بشكل فعال من فائدة هذه الخوارزمية المقترحة عن طريق أداة المحاكاة الرقمية باستخدام برمجية Simplorer، حيث إنّ النتائج المتحصل عليها بُينت أنّ هذه الخوارزمية المقترحة بإمكانها تحسين عمل نظام الطاقة الشمسية بشكل ملحوظ في أطوار التشغيل الثابتة والديناميكية.

1 Introduction

Photovoltaic (PV) power systems convert sunlight directly into electricity. A residential PV power system enables a homeowner to generate some or all their daily electrical energy demand on their own roof, exchanging daytime excess power for future energy needs (i.e., nighttime usage). The house remains connected to the electric utility at all times, therefore any power needed above what the solar system can produce is simply drawn from the utility. PV systems can also include battery backup or uninterruptible power supply (UPS) capability to operate selected circuits in the residence for hours or days during a utility outage [1].

The use of the solar energy is increasingly emphasized and regarded as a very important resource of power energy in the future. One of the main challenges for the PV industry is to increase the efficiency of PV conversion which varies severely with atmospheric conditions [2,3]. Therefore, it is necessary to concentrate our forces to reduce the application costs and to increment their performance. In order to reach the last aspect, it is important to note that the output characteristic of a PV array is nonlinear and changes with solar irradiation and cell's temperature. In general, for the output characteristic of a PV array there is an only point on the V–I or V–P curve, called the maximum power point (MPP), at which the entire PV system operates with maximum efficiency and produces its maximum output power. The location of the MPP is not known, but can be located, either through calculation models or by search algorithms.

The issue of MPPT to maintain the PV array's operating point at its MPP has been addressed in different ways in the literature; examples in [4–13]. In this work, our attention will be focused on an efficient MPPT algorithm used to maximize the PV array output power by tracking continuously the MPP, which depends on atmospheric conditions. The modeling of the system is realized using the novel concept of "functional prototyping" based on VHDL-AMS language, where the major advantage of this concept is that the models' behavior can be written in different levels of abstraction in mixed signal (analog–digital) and in mixed technology (electrical, mechanical, thermal, magnetic, etc.,), allowing designers to study and optimize the performance (verification) of components at different stages of the design process, before fabrication. The usefulness of the proposed MPPT algorithm is verified by digital simulation using Simplorer software package which is a simple graphical interface makes even complex models easy to design. Fast and stable simulation algorithms reduce simulation time and provide reliable results.

The remaining contents of this paper are organized as follows. Section 2 introduces the basic principle of the PV array mathematical modeling. Sections 3 and 4 describe the basic MPPT operating principles and the proposed MPPT algorithm for a PV module connected to a lead–acid battery, respectively. Section 5 describes the VHDL-AMS prototyping for principal parts of the PV power system. Section 6 discusses the obtained simulation results using Simplorer software in steady and dynamic states. Conclusions are finally drawn in the last section.

2 PV Array Mathematical Modeling

A PV array is a set of PV cells, connected together in serial or in parallel way or in a combination of them. Most solar modules are currently produced from silicon PV cells. These are typically categorized as monocrystalline or polycrystalline modules. In our case, the used PV power system is based on polycrystalline module, with regard to the behavior of a real solar cell, two parasitic resistances inside the cell, series R_S and parallel resistance R_P are taken into consideration as indicated in the equivalent circuit diagram in Fig. 1. The series resistance R_S arises from the bulk resistance of the silicon wafer, the resistance of the metallic contacts of the front and back surface and further circuit resistances from connections and terminals. The parallel resistance R_P is mainly caused by leakage currents due to *p-n* junction non-idealities and impurities near the junction, which cause partial shorting of the junction, particularly near the cell edges.

From Fig. 1, we deduce the Eq. (1) which describes the current–voltage characteristics of the PV cell depending on light-generated current [9–11]:

$$I_{\text{cell}} = I_{\text{ph}} - I_S\left(\exp\left(\frac{qV_D}{nKT_c}\right) - 1\right) - \frac{V_{\text{cell}} + I_{\text{cell}}R_S}{R_P} \tag{1}$$

where, I_{ph}, light-generated current (A); V_D, voltage across the diode (V); I_S, reverse saturation current (A); q, electron charge (C); K, Boltzmann constant (ev); n, ideality factor (n = 2); T_c cell temperature in Kelvin (K); R_S, solar cell series resistance [Ω]; R_P, solar cell parallel resistance[Ω].

Figure 2 shows the electrical characteristics of the PV cell.

The PV cell characteristics present three important points: the short circuit current I_{sc} ($I_{sc} \approx 4.5$ A), the open-circuit voltage V_{oc} ($V_{oc} \approx 0.6$ V), and the optimum power P_{op} ($P_{op} \approx 2.2$ W) delivered by the PV array to an optimum load R_{op} when the PV cells operate at their MPP.

On the other hand, the generated current is deeply depending on the captured radiation, from which it may be assumed that the relation which associates between light-generated current (I_{ph}) and the captured solar irradiation is given in Eq. (2):

$$I_{\text{ph}} = (I_{sc} \cdot I_r / I_{r\_stc}) \tag{2}$$

where I_r is the solar panel incident irradiation, I_{sc} is the short circuit current and I_{r_stc} is the irradiation at standard test condition (STC) (Irradiance: 1,000 W/m^2 and cell temperature: 25 °C).

Figure 3 shows the current–voltage and power–voltage characteristics of a PV cell for different values of solar radiation.

As shown in Fig. 3a, b, the short-circuit current is clearly proportional to the solar radiation, more radiation implies more current and more generated power.

Substituting (2) into (1), we obtain:

$$I_{\text{cell}} = \frac{I_{sc} \cdot I_r}{I_{r\_stc}} - I_S\left(\exp\left(\frac{qV_D}{nKT_c}\right) - 1\right) - \frac{V_{\text{cell}} + I_{\text{cell}}R_S}{R_P} \tag{3}$$

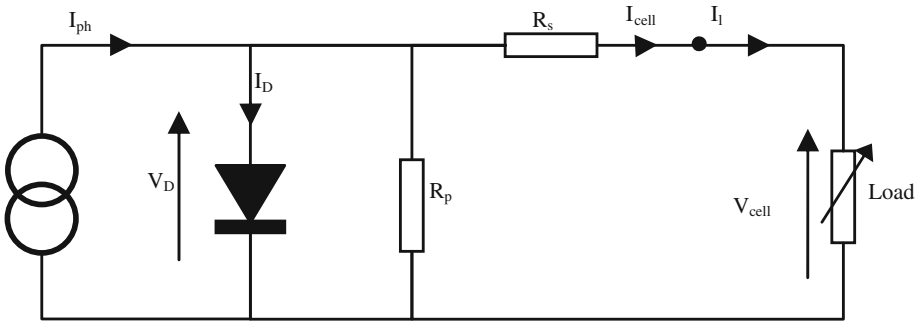

Fig. 1 PV cell equivalent circuit

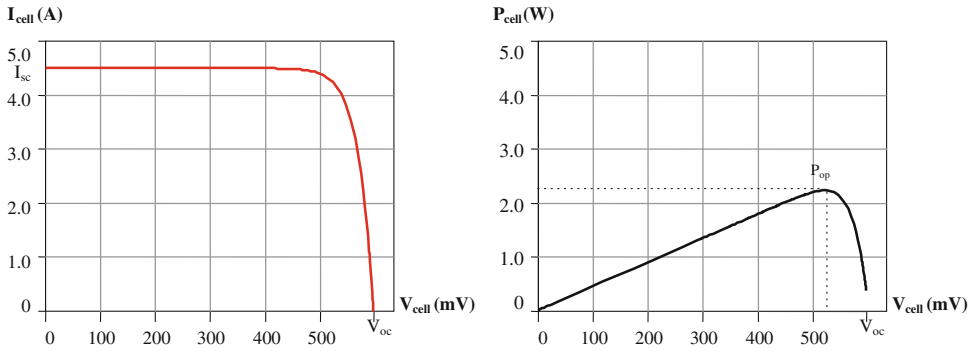

(a) Current-Voltage characteristic. **(b)** Power-Voltage characteristic.

Fig. 2 Electrical characteristics of the PV cell

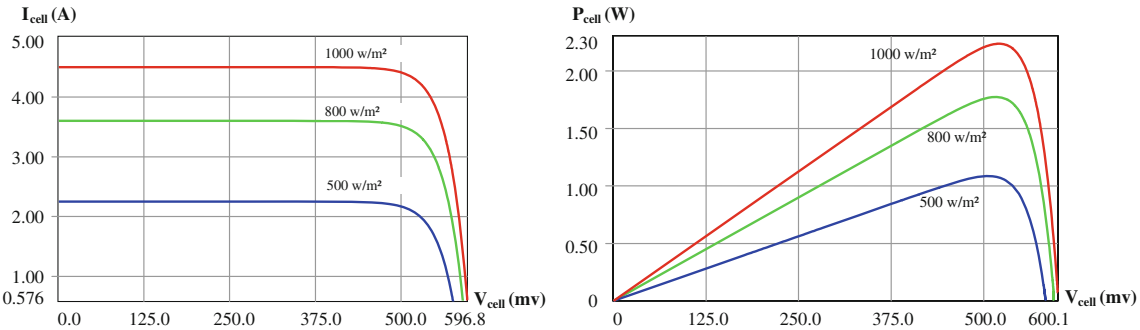

(a) Current-Voltage characteristics. **(b)** Power-Voltage characteristics.

Fig. 3 Effects of different irradiations on the PV cell

Then, (4) describes the effect of Ns PV cells connected in serial and N_p PV cells connected in parallel.

$$I_{pv} = N_p I_{cell} \text{ and } V_{pv} = N_s V_{cell} \tag{4}$$

where, N_S, number of cells connected in series; N_P, number of cells connected in parallel; V_{pv}, PV array voltage; I_{pv}, PV array current.

From (1), (2), and (4), we can deduce the characteristics equation of N_s*N_p PV cells [12]:

$$I_{pv} = N_p\left[\frac{I_{sc}\cdot I_r}{I_{r\_stc}} - I_s\left(\exp\left(\frac{q}{nKT_c}\left(\frac{V_A}{N_s}+\frac{R_s\cdot I_{pv}}{N_p}\right)\right)-1\right)\right] - \frac{N_p\cdot V_{pv}}{N_s R_p} - \frac{R_s\cdot I_{pv}}{R_p} \tag{5}$$

The produced power for N_s*N_p PV cells is given by:

$$P_{pv} = I_{pv}\cdot V_{pv} = V_{pv}\cdot N_p\left[(I_{sc}\cdot I_r I_{r\_stc}) - I_s\left(\exp\left(\frac{q}{nKT_c}\left(\frac{V_{pv}}{N_s}+\frac{R_s\cdot I_{pv}}{N_p}\right)\right)-1\right)\right] - \frac{N_p\cdot V_{pv}^2}{N_s R_P} - \frac{R_s\cdot I_{pv}\cdot V_{pv}}{R_P} \tag{6}$$

(5) and (6) highlight the effect that can have environmental factors such as the variations of temperature and solar irradiation, and PV array structure on generated power.

3 MPPT Operating Principles

The purpose of the MPPT is to move the array operating point close to the MPP under changing atmospheric conditions. In

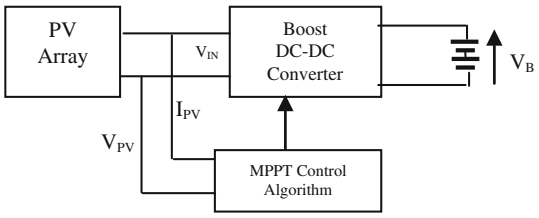

Fig. 4 PV power system with MPPT structure

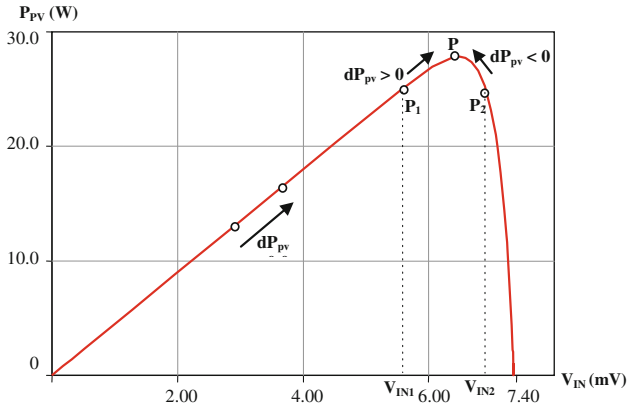

Fig. 5 Different PV panel operating points for different values of DC–DC converter input voltage

practice, optimal power load will be achieved through the use of a variable duty cycle of the control part of the MPPT converter, which controls directly the operating voltage which corresponds to this optimal load [6,7,9,10,14].

Figure 4 shows the basic fundamental block diagram of the full system, which consists of a PV array generator, a storage battery and a boost DC–DC converter inserted between the PV array and the storage battery. The boost DC–DC converter is piloted by a pulse-width modulation signal (PWM) which is provided by the MPPT control algorithm. The MPPT algorithm imposes the duty cycle D of the PWM signal as well as the PV panel operating point to extract the maximum power.

Figure 5 shows the different PV panel operating points for different values of DC–DC converter input voltage. The power flow is controlled by adjusting the duty cycle D of the provided PWM signal. It is noted that the operating points P_1 and P_2 correspond, respectively, to input voltages V_{IN1} and V_{IN2} or, respectively, to duty cycles D_1 and D_2.

In this case, the expression of V_{IN} is given by:

$$V_{IN} = V_B(1 - D) \tag{7}$$

where V_B is the battery voltage, and D is duty cycle.

The transition from P_1 to a generic point P is carried out by increasing the duty cycle as:

$$D_P = D_1 + \alpha \cdot t \tag{8}$$

where α is a positive constant, t is the time, and D_p is the duty cycle corresponding to point P.

In the same way, for a transition from P_2 to P, the duty cycle must be decreased. In this case, α changes its sign and becomes negative.

Therefore, the expression of the input voltage V_P corresponding to point P is given by:

$$V_P = V_B(1 - D_1 - \alpha \cdot t) \tag{9}$$

On the other hand, we can write:

$$V_{IN1} = V_B(1 - D_1) \tag{10}$$

Taking into account (9) and (10), we obtain:

$$V_P = V_{IN1} - V_B \cdot \alpha \cdot t \tag{11}$$

The derivative of the power P_{pv} delivered by the PV array with respect to duty cycle D is given by:

$$\frac{dP_{pv}}{dD} = \frac{dP_{pv}}{dV_{IN}} \frac{dV_{IN}}{dD} \tag{12}$$

Taking into account (7), (12) becomes:

$$\frac{dP_{pv}}{dD} = -V_B \frac{dP_{pv}}{dV_{IN}} \tag{13}$$

Hence,

$$\frac{d^2P_{pv}}{dD^2} = -VB \frac{d^2P_{pv}}{dV_{IN}^2} \frac{dV_{IN}}{dD} = V_B^2 \frac{d^2P_{pv}}{dV_{IN}^2} \tag{14}$$

At the MPP, we have $\frac{dP_{pv}}{dV_{IN}} = 0$.

This implies:

$$\frac{dP_{pv}}{dD} = 0 \tag{15}$$

Also at MPP:

$$\frac{d^2P_{pv}}{dV_{IN}^2} < 0 \tag{16}$$

This implies:

$$\frac{d^2P_{pv}}{dD^2} < 0 \tag{17}$$

From (15) and (17), we conclude that the PV array power is a concave function of the duty cycle.

4 Proposed MPPT-Based Solar System

All parts of the designed PV power system are assembled in the architecture shown in Fig. 6. This illustration details the links between power subsystem, sensors, and MPPT controller.

The power P_{pv} of the PV module is calculated by measuring the voltage and current of the PV array using voltage and current sensor models. Two delay blocks (τ_1 = 0.1 ms and τ_2 = 0.3 ms delay time) are used to detect variation of generated power. Then, the output comparator provides a digital

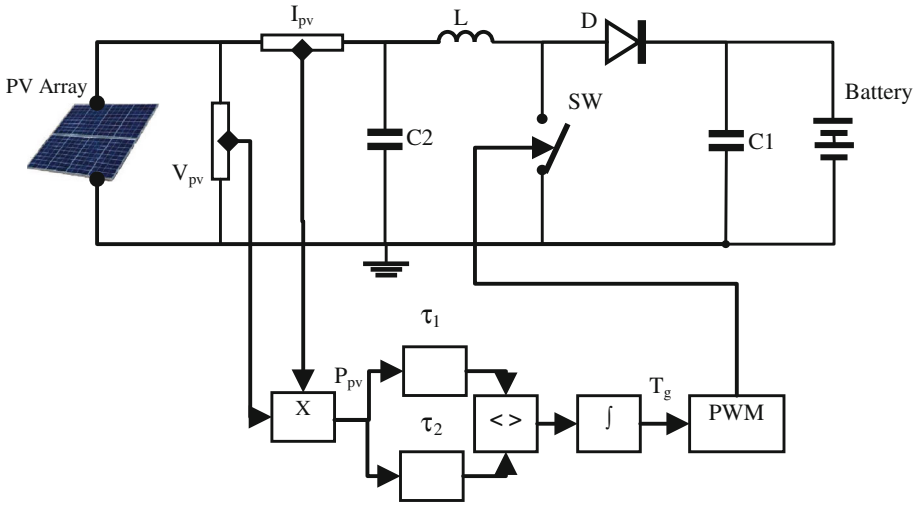

Fig. 6 Proposed architecture

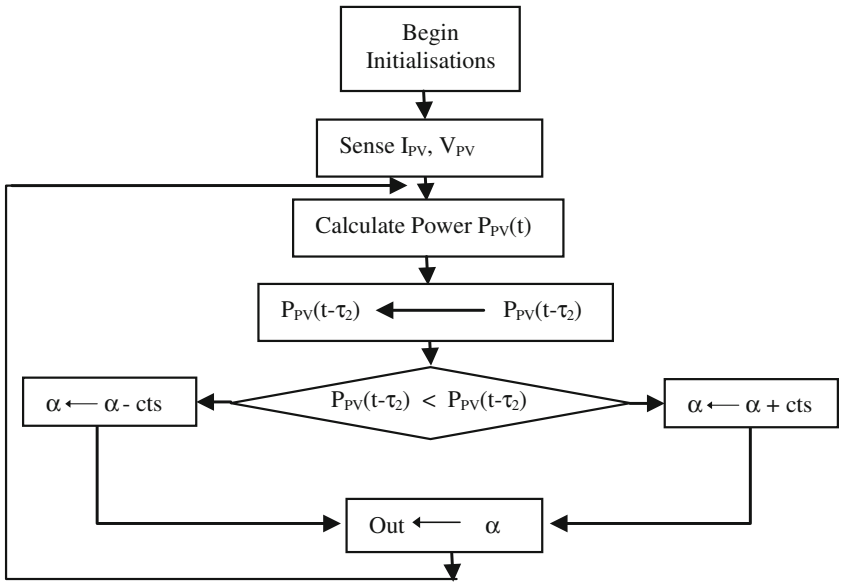

Fig. 7 Flowchart of the proposed control algorithm

signal which indicates whether the power time derivative is positive or negative. The digital signal is multiplied by a constant α to be integrated to form triangular signal T_g that will be the reference for the PWM algorithm.

The flowchart depicted in Fig. 7 shows how PWM signal of the proposed MPPT algorithm is produced. After calculating generated power, the duty cycle is estimated by comparing the power for two consecutive time; if the derivative power is positive the duty cycle will be increased and vice-versa.

During charging, the PV generator (12 serial cells) current flows through the diode *D* into the battery. As achieving the maximum charge voltage, the PV generator is short-circuited by the regulating unit, so that no more charging current can circulate. The diode prevents here, on one hand, the current reversal from the battery into this short-circuited path; on the other hand it prevents discharging of the battery to the unlighted PV generator at night.

5 VHDL-AMS Prototyping

The complexity of solar power systems urges toward efficient means for the co-design of digital, analog, and mixed signal blocks. System-level constraints must be propagated in the design flow down to the lower levels to trim device parameters.

The VHDL-AMS has been conceived for modeling not only analog and mixed-signal circuits, but also mixed-technology systems. It supports the use of digital constructs together with electrical quantities, differential equations and algebraic constraints. In addition, it allows the hardware description with different levels of abstraction, then making viable a top-down design methodology [15–18].

The VHDL-AMS modeling language gives designers an ability to model both internal and external system description and analyze each factor's effect on system performance.

```
library ieee;
use ieee.math_real.all;
use ieee.electrical_systems.all;

entity pv_module is
   generic(
        Rs  : real := 1.0e-5;
        Rp  : real := 1.0e+5;
        Isc  : real := 4.5;
        Is  : real := 1.0e-15;
        Vt   : real := 25.0e-3;
        );
   port(
        terminal p,m : electrical;
        quantity pw_inst : out real;
        );
end entity pv_module;

architecture arch_pv_module of pv_module is
       quantity Vcell across Icell through m to p;

begin
     Icell == Iph - Is * (exp((Vcell+Icell*Rs)/vt) -1.0 )
                -((Vcell+Icell*Rs)/Rp);
     pw_inst == -Icell*Vcell;
end architecture arch_pv_module;
```

Fig. 8 VHDL-AMS model of PV cell

In addition, the concept of functional prototyping which we used in our approach is a behavioral model methodology that considers the specifications and the characteristics earlier in the flow design, allowing designers to study and optimize the performance of components before fabrication. The developed functional prototype of the solar cell system and its MPPT algorithm allows the study and simulation of the PV cell performances which include: output voltage, efficiency, and generated power. In this section, we will discuss the principal parts of the system, which are the PV array, the storage battery and the boost DC–DC converter.

5.1 VHDL-AMS PV Cell

In order to realize the modeling of our system, we begin by designing of a functional prototype for the PV cell using the VHDL-AMS language. Different models can be made with various abstraction levels. A first VHDL-AMS description of the PV cell (Fig. 8) is used to reproduce the cell current–voltage and power–voltage characteristics, this model makes easy a parametric study of PV cell, it includes the library that makes the model useful, the used generics to characterize the PV cell and the ports (or pins) via which the model can be connected to other components.

Then, the final model is created by introducing all parameters of the solar array such as solar irradiance and PV cells number, also other parameters are added to guarantee a better hierarchical modeling methodology.

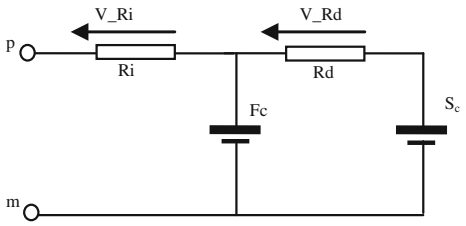

Fig. 9 Electronics equivalent circuit of the battery

5.2 VHDL-AMS Model of The Lead–Acid Battery

In a lead–acid battery, chemical energy is transformed to electrical energy at the battery electrodes through chemical reaction of the acid molecules with the electrode materials. The chemical reaction at the battery electrodes results in a lower concentrations of the lead–acid near the electrodes during discharge. The diffusion of the acid molecules between regions of high and low concentration is modeled with three models: the diffusion resistor R_d, a slow and a fast capacitor (F_C, S_C). Since the acid near the battery electrodes is consumed faster, its concentration is lower. This is modeled as a fast capacitor F_C that discharges quickly. The fast capacitor F_C that discharges quickly reproduces the lower concentration of the acid near the battery electrodes where is consumed faster.

The acid concentration farther from the electrodes is not consumed as fast, therefore it is modeled as a slow capacitor S_C that discharges slowly. The actual diffusion of the acid molecules between the regions of low and high concentrations is modeled with a diffusion resistor R_d. The electrical resistance of the electrodes is modeled as the internal resistance R_i of the battery.

The electronics equivalent circuit of the battery is shown in Fig. 9 [19,20].

The entity of the VHDL-AMS model of the battery behavior is shown in Fig. 10.

5.3 VHDL-AMS Model of DC–DC Converter

A basic topology of a PWM DC–DC boost converter is chosen to perform the power conversion from PV array to battery. It consists of controlled switch S, diode D, filter inductor L, and filter capacitor C.

The resistor, capacitor, inductor, and diode are the elementary electrical components that can be easily modeled using current–voltage relationship. Models written in VHDL-AMS can be as detailed as desired, including numerous effects beyond ideal behavior. However, we include only as much detail as it is necessary for the analysis being performed. With VHDL-AMS, we can write models with many degrees of detail by implementing several architectures in the model and using one at a time.

```
library ieee;
use ieee.math_real.all;
use ieee.electrical_systems.all;

entity  bat_soc is
generic (factor : real :=1.0;
          Ri      : real := 1.0e-2;
          Fc      : real := 60.0;
          Rd      : real := 4.0e-2;
          Sc      : real := 2.0e4;
          v_init  : real := 12.0;
          v_max : real := 14.0
          );
port( terminal  p, m      : electrical;
      quantity soc_out : out real :=0.0;
      quantity v_out    : out real :=0.0
      );
end entity bat_soc;
```

Fig. 10 VHDL-AMS entity of the battery model

```
entity switch is
   generic (ron   : real := 1.0e-3;
            roff  : real  := 1.0e6;
            ton   : real  := 1.0e-9;
            toff   : real := 1.0e-9
           );
   port (terminal p, m  : electrical;
         signal   sw_state : out bit
        );
end entity switch;
```

Fig. 11 VHDL-AMS entity of the switch model

The switch component will typically be a power bipolar transistor or power MOSFET. In the early design stages, we may not have determined which particular device to use. However, since we are only using the device as a switch, it will be either ON or OFF, therefore its detailed characteristics are not relevant. We can proceed with simulations of the system using an idealized model of the device. The behavioral model of the switch presented in Fig. 11 describes an ideal switch with transition effect, it can easily replace semiconductor switch in several applications as a sophisticated high power semiconductor and it presents a good convergence working.

The boost converter is then assembled in a structural model, which consists of a set of instantiated functional and behavioral models of capacitor, diode, inductor, and switch as shown in Fig. 12.

6 Simulation Results and Discussions

In order to verify the static and dynamic performances of the proposed MPPT algorithm and the reliability of VHDL-AMS

```
library ieee;
use ieee.math_real.all;
use ieee.electrical_systems.all;

entity tb_BoostConverter is
    port ( ctrl : std_logic
         );
end tb_BoostConverter;

architecture BoostConverter of tb_BoostConverter is
   terminal p1 : electrical;
   terminal p2 : electrical;
   terminal p3 : electrical;
begin
   L1 : entity work.inductor(ideal)
        port map ( p1 => p1, p2 => p2 );
   sw1 : entity work.switch(ideal)
        port map ( sw_state => ctrl, p1 => p2, p2 => electrical_ref);
   D1 : entity work.diode(ideal)
        port map ( A =>p2, K => p3 );
   C1 : entity work.capacitor(ideal)
        port map ( p1 => p3, p2 => electrical_ref );
end architecture BoostConverter;
```

Fig. 12 Structural VHDL-AMS code for the boost converter

prototype, the PV power system was simulated for constant irradiance and angle, then for variable irradiance and angle.

Our system was simulated on Simplorer which is a software package used to design and analyze complex technical systems. Simulation models created with Simplorer can contain circuit components from different physical domains, block elements, and state machine structures modeled in Simplorer modeling language (SML), as well as VHDL-AMS. Further, Simplorer performs calculations for simulation models described in VHDL-AMS. The SML compiler automatically starts the VHDL-AMS simulator if VHDL-AMS components are used in the simulation model. Standard components for VHDL-AMS simulation are available on the "AMS" tab, the "Digital" tab, and the "Tools" tab of the Model agent [21–23].

6.1 Steady-State Simulation

The PV power system is firstly tested without use the MPPT controller. The waveform of PV array power is presented in Fig. 13. We can observe that without MPPT controller, the PV array cannot work because the provided power is not stable around its maximum operating power points and decreases quickly to zero value, which shows that a MPPT technique is necessary, to extract the maximum power from the PV array.

The PV power system is operated using the proposed MPPT algorithm and simulated under steady-state solar irradiance and temperature conditions. The waveforms of PV array power (P_{pv}), PV array current (I_{pv}), PV array voltage (V_{pv}), and control triangular signal (T_g) are shown in Fig. 14. It is noted that the PV power system, using the proposed MPPT algorithm, is able to accurately track MPPs with

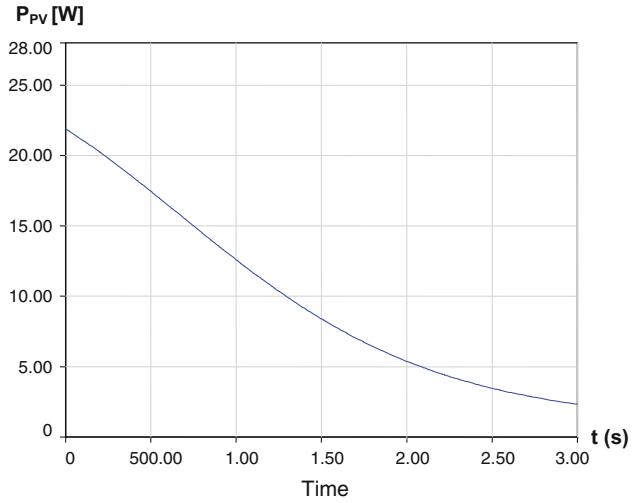

Fig. 13 Waveform of PV array power without MPPT controller

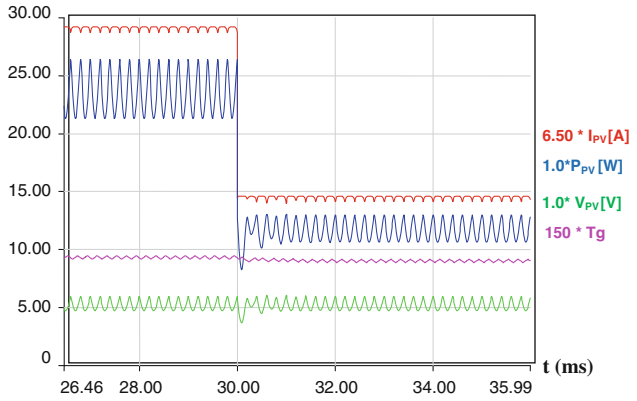

Fig. 15 Different waveforms of PV power system for rapidly changing irradiance

minimum steady-state power oscillations. It can be observed that the proposed MPPT controller in steady-state (as well shown in Fig. 14b) allows to bring back the power operating point quickly to a stable level of about 24 W at 1,000 W/m^2, keeping the PV array voltage and the PV array current to be stables around ($V_{pv} \approx 5.48$ V, $I_{pv} \approx 4.5$ A).

6.2 Dynamic Simulation

The proposed MPPT algorithm is tested under two different weather conditions, i.e., for rapidly changing irradiance and different tilt angles cases. The purposes of tests are to investigate the dynamic characteristics of PV power system using the proposed MPPT controller.

6.2.1 Rapidly Changing Irradiance Levels

The different waveforms of PV power system under step change in solar irradiance values from 1,000 W/m^2 to 500 W/m^2 are illustrated in Fig. 15. In the first case (for 1,000 W/m^2), the averages PV array current and power are very close to their optimal values of ($I_{pv} \approx 4.5$ A, $P_{pv} \approx 24$ W), respectively. In the second case, when irradiation level is decreased to 500 W/m^2 at time 30 ms, it is shown clearly, that after a short transient, the PV array current and power are adjusted to the new optimal values, which are ($I_{pv} \approx 2.24$ A, $P_{pv} \approx 13$ W), and the PV array voltage remains constant. This test demonstrates that the proposed MPPT controller has the ability to accurately track MPP with minimum power ripples.

In order to show clearly the response of the PV power system during the dynamic state for a rapidly changing irradiance, the zoomed waveforms of both PV array current and voltage are shown in Fig. 16, respectively.

Figure 17 shows the characteristics of PV array P_{pv} (V_{pv}) and P_{pv} (I_{pv}) for different levels of irradiance, respectively. The irradiance is increased from 500 W/m^2 to 1,000 W/m^2 with a rate of 100 W/m^2. It can be observed that the proposed MPPT controller ensures a maximum power operating point for any level of irradiance, therefore an increase in irradiance produces an increase in PV array current and consequently an increase in PV array power, but the PV array voltage is

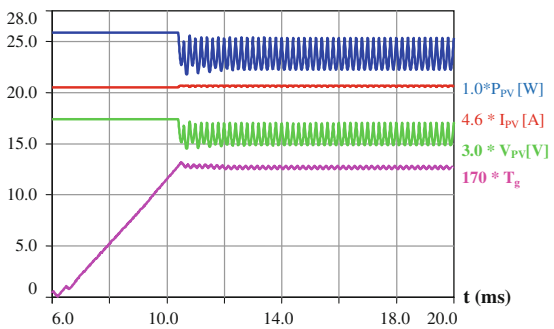

(a) Different waveforms of PV power system.

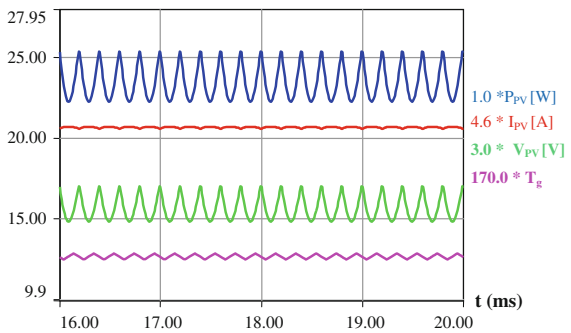

(b) Zoomed waveforms of PV power system in steady-state.

Fig. 14 Simulation results under steady-state solar irradiance and temperature conditions

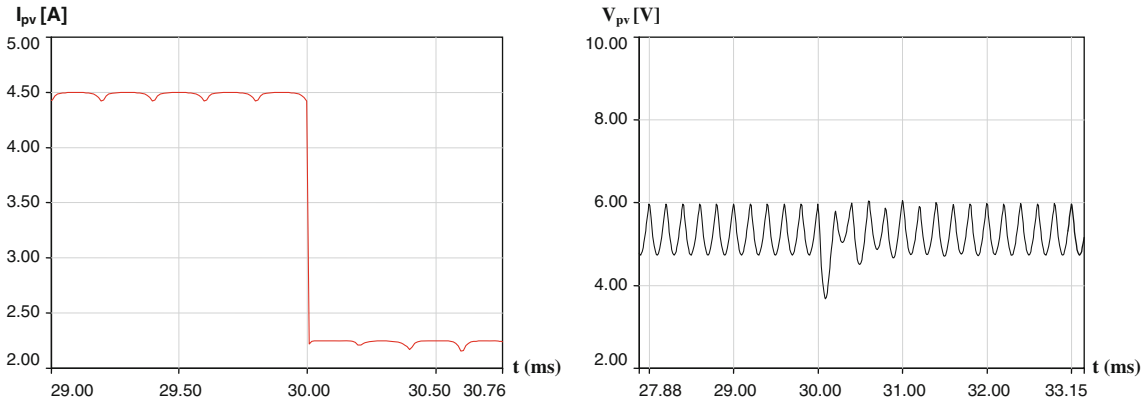

(a) PV array current waveform. **(b)** PV array voltage waveform.

Fig. 16 Zoomed waveforms of PV array current and voltage for step change on irradiance

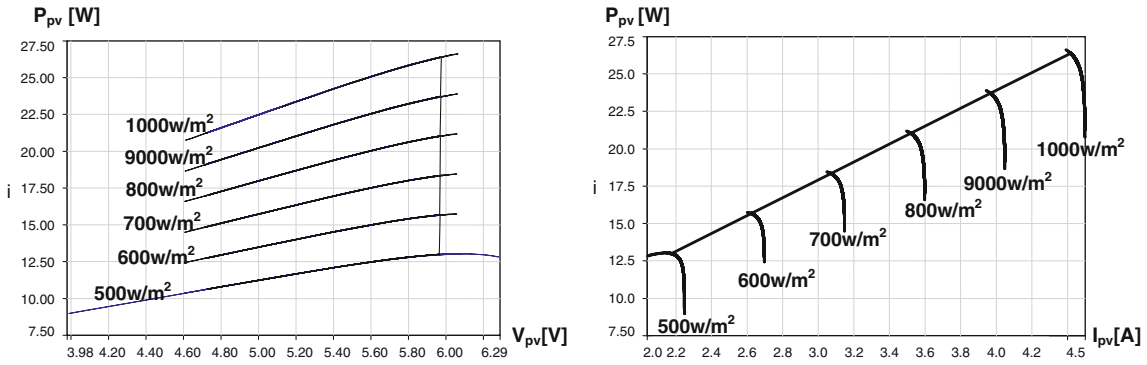

(a) PV array power-voltage. **(b)** PV array power-current.

Fig. 17 Characteristics of PV array for step changes on irradiance

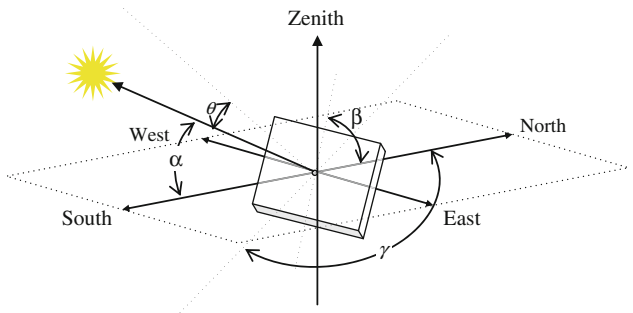

Fig. 18 Defining PV module angles

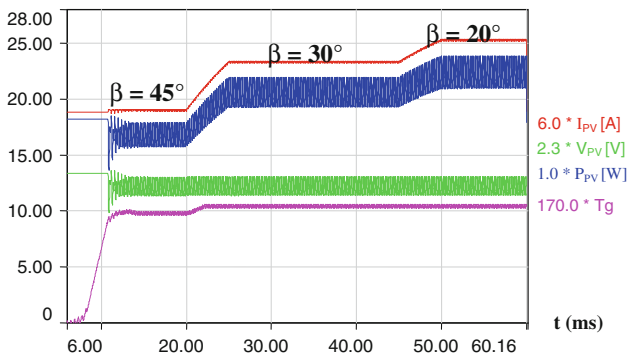

Fig. 19 Waveforms of PV power system for different tilt angles

still unchanged for any maximum power operating points, because the voltage is the result of ration of power by current.

6.2.2 Response Under Different Tilt Angles

Usually, a PV array is integrated into a solar tracking system to extract the maximum energy from the sun. For this, to demonstrate the efficiency of the proposed MPPT algorithm, we consider that the PV array is placed at different tilt angles β to the horizon. The system can be simulated by rotating the PV array around the east west axis, as shown in Fig. 18.

The variation in the tilt angle implies a change of the incident irradiation received by the solar panel, therefore the direct incident irradiation is given by [24]:

$$I_r = I_{rrad} \cos(\theta) \tag{18}$$

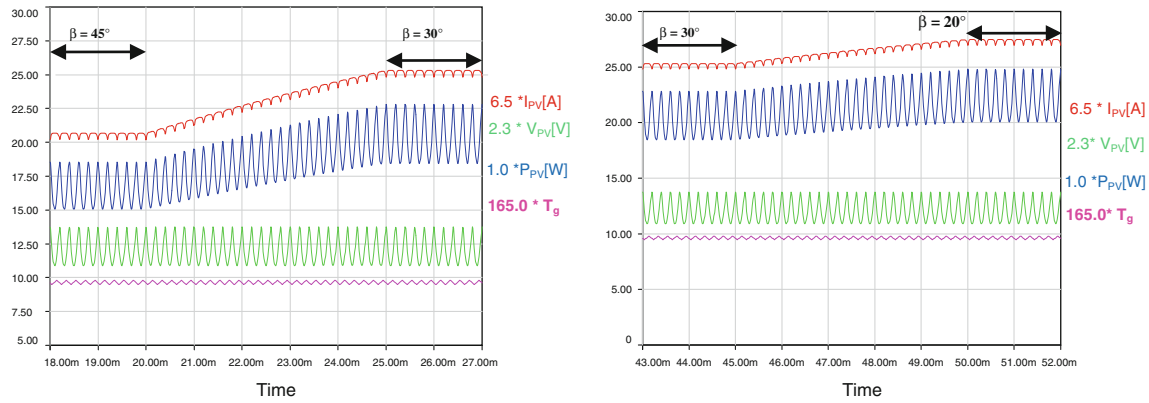

(a) From β=45° to β=30°. **(b)** From β=30° to β=20°.

Fig. 20 Zoomed waveforms of PV array for different tilt angles

Table 1 Power extracted under different tilt angles

Tilt angle β (°)	45	30	20
Power (W)	17.3	21.0	23.7
Current (A)	3.16	3.83	4.33
Voltage (V)	5.48	5.48	5.48

The equation of the incidence angle is given by:

$$\cos(\theta) = (\sin(\sigma) \cdot \cos(\beta)) + (\cos(\sigma) \cdot \sin(\beta) \cdot \cos(\gamma - \mathrm{A})) \tag{19}$$

where A, solar azimuth angle; σ, solar altitude angle; β, solar panel tilt angle; γ, surface azimuth angle; θ, Incidence angle.

The PV array current is given by (20) which takes into consideration the incident angle of the PV panel.

$$I_{\mathrm{PV}} = N_{\mathrm{p}}\left[\frac{I_{\mathrm{sc}} \cdot I_{\mathrm{rrad}} \cdot \cos(\theta)}{I_{\mathrm{r\_stc}}} - I_{\mathrm{s}}\left(\exp\left(\frac{q}{nKT_{\mathrm{c}}}\left(\frac{V_{\mathrm{PV}}}{N_{\mathrm{s}}} + \frac{R_{\mathrm{s}} \cdot I_{\mathrm{PV}}}{N_{\mathrm{p}}}\right)\right) - 1\right)\right] - \frac{N_{\mathrm{p}} \cdot V_{\mathrm{PV}}}{N_{\mathrm{s}} R_{\mathrm{p}}} - \frac{R_{\mathrm{s}} \cdot I_{\mathrm{PV}}}{R_{\mathrm{p}}} \tag{20}$$

Figure 19 shows the system responses after variation in the tilt angle. This is done by changing this angle in the PV array model several times during simulation and by fixing sun position at zenith ($A = 180°$ and $\alpha = 90°$) for constant irradiance 1,000 W/m^2. For any position of the panel (variation on tilt angle), the PV array voltage remains unchanged, and we can observe that the proposed MPPT algorithm keeps its effectiveness and tracks quickly the maximum power operating point for any tilt angle.

In order to show clearly the responses of the PV power system during the dynamic state for different tilt angles. The different waveforms presented in Fig. 19 are zoomed and shown in Fig. 20.

Table 1 shows the average values of PV array power, current and voltage; respectively, these values are obtained for constant irradiance 1,000 W/m^2 and for different tilt angles 45°, 30°, and 20°.

7 Conclusions

This paper has presented an improved MPPT algorithm used to maximize the PV array output power by tracking continuously the MPP which depends on atmospheric conditions (panel temperature and irradiance). The PV power system is modeled using the novel concept of "functional prototyping" based on VHDL-AMS language and simulated on Simplorer software. The obtained simulation results showed that the proposed MPPT algorithm is able to accurately track MPP with minimum power oscillations and it has proved itself to be quite satisfactory, considering both transient and steady state system.

In this work, we showed how a high-level language can be used to model such complex system multi-technological energy system gathering several disciplines at the same time, and we also showed that using various levels of abstraction from structural to functional level can make the design more intelligible and more compliant.

This work presents a significant first step in developing VHDL-AMS models of PV power systems and more generally of any renewable energy systems. The final objective is to elaborate a complete library to give engineers a valuable tool and a low cost platform for designing and validating system at different levels of details and abstraction.

References

1. Roger, A.: Messenger Jerry Ventre.: Photovoltaic systems engineering. 2nd edn. CRC press, New York (2004)
2. Esram, T.; Chapman, P.L.: Comparison of photovoltaic array maximum power point tracking techniques. IEEE Trans Energy Convers. **22**(2), 439–449 (2007)
3. Dolara, A.; Faranda, R.; Leva, S.: Energy comparison of seven MPPT techniques for PV systems. J. Electromagn. Anal. Appl. **3**, 152–162 (2009)

4. Jancarle L.; et al.: A maximum power point tracker for PV systems using a high performance boost converter. Solar Energy. **80**(7), 772–778 (2006)
5. Salas, V.; OlIas, E.: Review of the maximum power point tracking algorithms for stand-alone photovoltaic systems. Solar Energy Mater. Solar Cells. **90**(11), 1555–1578 (2006)
6. Chao, R.M.; et al.: Evaluation of a photovoltaic energy mechatronics system with a built-in quadratic maximum power point tracking algorithm. Solar Energy. **83**, 2177–2185 (2009)
7. Chowdhury, S.R.; Saha, H: Maximum power point tracking of partially shaded solar photovoltaic arrays. Solar Energy Mater. Solar Cells. **94**(9), 1441–1447 (2010)
8. Altas, I.H.; Sharaf, A.M.: A novel maximum power fuzzy logic controller for photovoltaic solar energy systems. Renew. Energy. **33**, 388–399 (2008)
9. Tafticht, T.; et al.: An improved maximum power point tracking method for photovoltaic systems. Renew. Energy. **33**(7), 1508–1516 (2008)
10. Rodriguez, C.; Gehan A.; Amaratunga, J.: Analytic solution to the photovoltaic maximum power point problem. IEEE Trans. Circuit Syst. **54**(9) (2007)
11. Benmessaoud, M.T.; et al.: New approach modeling and a maximum power point tracker method for solar cells. Comput. Math. Appl. **60** 1124–1134 (2010)
12. Dali, M.; Belhadj, J.; Roboam, X.: Design and energy based model of stand-alone hybrid photovoltaic-wind generating system with integration of converter losses. In: International conference on electrical engineering design & technologies, Hammamet, November (2007)
13. Zhou, S; et al.: Novel maximum power point tracking algorithms for stand-alone photovoltaic system. Int. J. Control Autom. Syst. **8**(6), 1364–1371 (2010)
14. Rashid, M.H.: Power Electronics Handbook. Academic Press, San Diego (2001)
15. Hérve, Y: VHDL-AMS; applications et enjeux industriels; cours et exercices corrigés. Dunod (2002).
16. Ashenden, P.J.; Peterson, G.D.; Teegarden, D.A.: The system designer's guide to VHDL-AMS: analog, mixed-signal and mixed-technology modeling. Morgan kaufmann publishers, San Francisco (2003)
17. IEEE, 1076.1.1 IEEE standard VHDL analog and mixed-signal extensions. Packages for multiple energy domains support, IEEE Computer society June (2005)
18. Hérve, Y; Desgreys, P.: Functional virtual prototyping design flow and VHDL-AMS. In: Forum on design languages, pp. 69–76. FDL'06, Darmstadt (2006)
19. Jossen, A.; et al.: Hybrid systems with lead–acid battery and proton-exchange membrane fuel cell. J. Power Sourc. **144**, 395–401 (2005)
20. Van Mierlo, J.; Van den Bossche, P.; Maggetto, G.: Models of energy sources for EV and HEV: fuel cells, batteries, ultracapacitors, flywheels and engine-generators. J. Power Sourc. **128**, 76–89 (2004)
21. SIMPLORER® 7.0 VHDL-AMS Tutorial. http://www.fbeit.htwk-leipzig.de
22. SIMPLORER® 7.0 Getting Started 2006. http://www.ansoft.com
23. Simulation system SIMPLORER® 6.0 Getting started, English edition, © 1996–2002, Ansoft Corporation
24. Armstrong, S.; Hurley, W.G: Investigating the effectiveness of maximum power point tracking for a solar system. In: Power electronics specialists conference, pp. 204–209 (2005)